Convergent Connectivity and Graded Specialization in the Rostral Human Temporal Lobe as Revealed by Diffusion-Weighted Imaging Probabilistic Tractography

Richard J. Binney, Geoffrey J. M. Parker, and Matthew A. Lambon Ralph

Abstract

■ In recent years, multiple independent neuroscience investigations have implicated critical roles for the rostral temporal lobe in auditory and visual perception, language, and semantic memory. Although arising in the context of different cognitive functions, most of these suggest that there is a gradual convergence of sensory information in the temporal lobe that culminates in modality- and perceptually invariant representations at the most rostral aspect. Currently, however, too little is known regarding connectivity within the human temporal lobe to be sure of exactly how and where convergence occurs; existing hypotheses are primarily derived on the basis of cross-species generalizations from invasive nonhuman primate studies, the validity of which is unclear, especially where language function is concerned. In this study, we map the connectivity of the human rostral temporal lobe in vivo for the first time using diffusion-weighted imaging probabilistic tractography. The results indicate that convergence of sensory information in the temporal lobe is in fact a graded process that occurs along both its longitudinal and lateral axes and culminates in the most rostral limits. We highlight the consistency of our results with those of prior functional neuroimaging, computational modeling, and patient studies. By going beyond simple fasciculus reconstruction, we systematically explored the connectivity of specific temporal lobe areas to frontal and parietal language regions. In contrast to the graded within-temporal lobe connectivity, this intertemporal connectivity was found to dissociate across caudal, mid, and rostral subregions. Furthermore, we identified a basal rostral temporal region with very limited connectivity to areas outside the temporal lobe, which aligns with recent evidence that this subregion underpins the extraction of modality- and context-invariant semantic representations. ■

INTRODUCTION

In his seminal review, Mesulam (1998) proposed that cognitive function and conscious experience arise from convergent patterns of connectivity and gradual integration of information. Similar ideas to this "graded convergence" principle can be found in both the sensory and cognitive neuroscience fields. In sensory neuroscience, it is broadly accepted that the visual (Felleman & Van Essen, 1991) and auditory (Rauschecker & Scott, 2009) ventral "what" pathways are hierarchically organized. In both modalities, there is a caudal–rostral gradient of feature convergence along which neuronal responses are increasingly tuned toward complex stimuli and away from low-level sensory variation resulting in the development of invariant representations that deal with irrelevant changes in perceptual quality, noise, source, etc. (e.g., Rauschecker & Scott, 2009; Deco & Rolls, 2004). Furthermore, advances in tracing neural connections in the nonhuman primate brain have led to the identification of several polysensory association areas, provoking renewed discussion of the importance of the convergence of information from different modalities for higher cognitive function (Mesulam, 1998; Pandya & Seltzer, 1982). Indeed, one such region—the rostral temporal lobe—has been proposed as a transmodal representational hub for the extraction of coherent concepts (Visser & Lambon Ralph, 2011; Binney, Embleton, Jefferies, Parker, & Lambon Ralph, 2010; Lambon Ralph, Sage, Jones, & Mayberry, 2010; Pobric, Jefferies, & Lambon Ralph, 2010; Patterson, Nestor, & Rogers, 2007). Related insights from computational modeling further suggest that the proposed function of this region might also arise from a graded convergence process (see Plaut, 2002; Discussion). These proposals are all based on the assumption—untested in humans—that convergent function follows from the pattern of underlying white-matter connectivity. The purpose of the current study, therefore, was to utilize diffusion-weighted imaging (DWI) probabilistic tractography to map the connectivity of the human rostral temporal lobe in vivo for the first time.

Detailed study of the white matter connectivity of the human temporal lobe has the potential to provide unique

University of Manchester

insights into the mechanisms that underlie such integrative processes. Specifically, understanding how each of the different temporal lobe regions is interconnected with one another may facilitate claims regarding how and where sensory information converges. Currently, however, very little is known regarding interregional connectivity within the in vivo human temporal lobe (Mesulam, 1998). This is primarily due to the limitations of the techniques traditionally used to explore the anatomy of the cerebral white matter. Postmortem fiber dissection using the Klingler freeze–thaw technique (Klingler & Gloor, 1960) involves peeling away the white matter tracts to reveal their structure in three dimensions. Since the 17th century, this technique has been instrumental in the identification of all the major fasciculi. Being limited to the level of bundles rather than single fibers, however, it provides a description of the overall trajectory of a tract but does not allow for precise or accurate determinations of beginning and end points. Moreover, revealing one tract necessarily means damaging another, including u-fibers. The vast majority of detailed information regarding directed long-distance interregional connections comes from invasive tract-tracing studies of the nonhuman primate brain (Schmahmann & Pandya, 2006; Felleman & Van Essen, 1991; Morán, Mufson, & Mesulam, 1987; Jones & Powell, 1970; Pandya & Kuypers, 1969). Considered a gold standard for assessing brain connectivity, this technique involves the injection of a tracer substance that is actively incorporated through the neuronal membrane and transported along the axon such that it becomes maximally concentrated in and thus labels cells within connected regions. This allows for quantification of the number of fibers connecting the injection site with a given brain structure so that comparisons between different labeled regions can be made. The technique is also informative with regard to which is the afferent or efferent brain structure. Unfortunately, the course of axonal projections is not clearly labeled, and thus it is not possible to uncover the route by which such brain regions are connected. More critically, the invasive nature of these techniques restricts their application to a limited number of experimental animals and there are always questions of generalizability when extending nonhuman primate findings to the human brain—particularly where language function is concerned (Gloor, 1997). Indeed, it is not yet absolutely clear as to what extent temporal lobe connectivity in monkey and human is similar, especially toward the more rostral cortices and due to the absence of a homologue of the human middle temporal gyrus. Furthermore, because of limits on the number of injection sites per specimen and the number of specimens available to such nonhuman primate research, a significant proportion of temporal lobe connectivity has yet to be established with this technique (see, e.g., the review of Felleman & Van Essen, 1991).

DWI tractography offers an unprecedented noninvasive, in vivo method for systematically exploring the connectivity of multiple sites both within and across human individuals, albeit at a much lower resolution than tracer-based methods ($\sim$2 mm^3). Tractography is different to the more commonly reported DWI-based measures, such as fractional anisotropy. Like structural (T1-weighted) data, these voxel-based measures are often used to compare between groups of subjects or to assess an association between this measure and clinical/performance variables. DWI tractography, on the other hand, is used to determine paths for anatomical connection between regions in the brain and it has been successfully used to reconstruct the major association fasciculi (Makris et al., 2009; Catani & de Schotten, 2008; Parker et al., 2005) that were first identified with the post-mortem fiber dissection techniques (above).

There are two main approaches to DWI tractography, the deterministic (or linear) and the probabilistic (or distributed) methods. Linear methods typically use the principal eigenvector of the diffusion tensor in each voxel (estimated from the DWI) as a propagation direction for the path of a "streamline" originating from a "seed" voxel. In its simplest form, this can be thought of as "linking a chain" of voxels, tracing from point to point, to produce a single white matter pathway that proceeds from the seed and through the tracts to its destination. Although relatively quick to compute, such linear methods are particularly susceptible to errors in the intravoxel orientation information due to the presence of noise in the data or where a voxel contains more than one tract direction implying crossing or branching fiber bundles. Moreover, they do not provide any estimate of the certainty of the existence of a pathway, and so erroneous pathways are attributed with as much significance as "true" pathways.

Recently, there has been an emergence of more sophisticated algorithms for interpreting DWI data that, unlike the diffusion tensor model (diffusion tensor imaging), account for realistic levels of noise and allow the presence of multiple intravoxel fiber orientations to be identified. These include diffusion spectrum imaging (Schmahmann et al., 2007) and high angular resolution diffusion imaging (e.g., constrained spherical deconvolution, Jeurissen, Leemans, Jones, Tournier, & Sijbers, 2011, or Q-ball imaging, Tuch, 2004). Probabilistic tractography methods aim to exploit this additional information to generate distributed probability maps of the white matter pathways between a seed region and all other voxels in the brain. One such approach (Parker & Alexander, 2005) is to simulate the diffusion process using a grid-based random walk in which a particle is allowed to diffuse through the brain, randomly sampling the orientation(s) of fiber populations within each voxel as they are encountered. This continues until some stopping criterion is reached and each voxel encountered on the random walk is noted. Repeating this process a large number of times in a Monte Carlo process generates a whole-brain map containing voxel-wise estimates of the probability of a white matter pathway existing between the start point and that voxel (the number of times it was encountered over all randomizations of the random walk). Although much more computationally

demanding and time-consuming, such methods more adequately account for crossing fibers and instances of branching tracts.

There are, in fact, two main ways in which probabilistic tractography can be implemented. The first, constrained probabilistic tractography, includes the definition of an endpoint (or target). In essence, this is similar to deterministic tractography, but instead of revealing only the single most likely pathway, it allows for the visualization of alternative trajectories of the hypothesized pathway connecting two regions and provides probability values pertaining to which is most likely to be anatomically correct. In this study, we used the alternative method, unconstrained probabilistic tractography, in which no single target is defined and multiple pathways are tracked out of the seed region regardless of their termination point. Thus, the output is a distributed map of multiple brain-wide pathways and contains probability estimates of how likely it is that different regions are connected to the seed point. These probability estimates can then be evaluated relative to each other and, ultimately, a more complete profile of the seed region's brain-wide connectivity can be scrutinized (see Methods). To be absolutely clear, we should note that, unlike the invasive tracer methods described above, this technique does not reveal "connections" but instead assesses the confidence of the presence of white matter routes or pathways via which two brain regions are possibly (but not necessarily) connected by monosynaptic axonal projections. Therefore, from herein, we shall only refer to "pathways" when discussing our data.

DWI tractography is currently the best noninvasive method by which white matter "connectivity" can be explored in the human brain in vivo and has been validated against invasive methods in the pig brain (Dyrby et al., 2007). However, the most recent innovations of DWI tractography methods have yet to be extensively applied in the human brain, most notably within the rostral temporal cortices. In this study, therefore, we used high angular resolution diffusion imaging probabilistic tractography to map white matter within the left human temporal lobe for the first time, with emphasis placed on connectivity of the more rostral cortices. We also incorporated a recent methodological advance that has overcome the signal dropout and image distortion that occurs within anteroventral temporal structures (see Methods; Embleton, Haroon, Morris, Lambon Ralph, & Parker, 2010; Visser, Embleton, Jefferies, Parker, & Lambon Ralph, 2010; Haroon, Morris, Embleton, Alexander, & Parker, 2009; Parker & Alexander, 2005).

Our second target relates to the known role of the left temporal lobe in language processing. Specifically, we sought to examine connectivity of this brain structure with ipsilateral frontal and parietal sites that are classically associated with language. Our intention was not simply to reconstruct the fasciculi that project to/from the temporal lobe, as this has already been done in a number of pioneering DWI tractography studies (Makris et al., 2009; Saur et al., 2008; Catani, Jones, & Ffytche, 2005). Instead, we mapped the differential connectivity of these classical fronto-parietal language areas to caudal, mid, and rostral temporal lobe regions. To the best of our knowledge, there have been no previous attempts to use DWI tractography to map these simultaneously, yet such information has the potential (a) to provide a more precise characterization of the temporal lobe's association pathways by identifying the specific temporal lobe subregions that are associated with each and (b) to generate hypotheses regarding the role of specific temporal lobe subregions in language processing.

METHODS

The imaging techniques, mathematical models, and applications of DWI tractography are becoming increasingly sophisticated, evermore precise and reliable. Adopting advanced methodologies, including a model-based residual-bootstrapped constrained spherical deconvolution algorithm and the probabilistic index of connectivity (PICo) software (Jeurissen et al., 2011; Haroon et al., 2009; Tournier et al., 2008; Parker & Alexander, 2005), was critical for achieving the standards required by the aims of this study. Of particular note was the use of a new combined imaging/correction method that has been developed to overcome signal dropout and geometric image distortions that arise in areas of high magnetic susceptibility variation and typically lead to failed or erroneous fiber tracking (Embleton et al., 2010; Visser et al., 2010). These image artifacts are particularly pronounced within the OFC and the polar and anteroventral temporal cortex, such that these regions have been inaccessible to many previous DWI tractography studies. Incorporating this new method was crucial for our aim of obtaining data from across the entire human temporal lobe. Each of the above-mentioned techniques and methodologies are reported in full elsewhere but are described briefly in the sections below.

Participants

Thirteen healthy participants (four women; mean age = 23.3 years, range = 19–37 years) took part. All were right-handed, yielding a laterality quotient of at least 80 on the Edinburgh Handedness Inventory (Oldfield, 1971). The research was approved by the local ethics board.

MRI Acquisition

All imaging was performed on a 3-T Philips Achieva scanner (Philips Medical Systems, Best, the Netherlands) using an eight-element SENSE head coil. Diffusion weighted images were acquired using a method designed to minimize problems associated with the inferior–anterior and polar aspects of the temporal lobe (Embleton et al., 2010; Visser et al., 2010). Specifically, DWI was performed using a pulsed gradient spin-echo EPI sequence including 60 contiguous slices covering the whole brain and with

echo time = 59 msec, repetition time ≈ 11,884 msec (variable due to cardiac gating; see below), $G = 62$ mT m^{-1}, half scan factor = 0.679, 112 × 112 image matrix reconstructed to 128 × 128 using zero padding, reconstructed resolution = 1.875 × 1.875 mm, slice thickness = 2.1 mm, 61 noncollinear diffusion sensitization directions at $b = 1200$ sec mm^{-2} (Δ, δ = 29.8, 13.1 msec), 1 at $b = 0$, and a SENSE acceleration factor = 2.5. Acquisitions were cardiac gated using a peripheral pulse unit positioned over the participant's index finger ($n = 10$) or an electrocardiograph ($n = 3$) to reduce artifacts associated with pulsatile movements in the brain (Jones & Pierpaoli, 2005). With this imaging protocol, we achieved an estimated signal-to-noise ratio of 35 in the $b = 0$ images and 29 in the diffusion-weighted volumes before distortion correction (the estimation included 10 axial slices and compared the average signal across all brain tissue with that of nonzero signal outside the head). Each diffusion weighted volume was acquired entirely before starting on the next diffusion weighting resulting in 62 temporally spaced volumes with different direction diffusion gradients. For each gradient direction, two separate volumes were obtained with opposite polarity *k* space traversal and hence reversed phase and frequency encode direction. One complete set of diffusion images was acquired with one direction *k* space traversal (left–right) and a second set of images then acquired with opposite direction traversal (right–left). Total imaging time was around 36 min, dependent on each subject's heart rate. A colocalized T2 weighted turbo spin echo scan with in-plane resolution of 0.94 × 0.94 mm and slice thickness 2.1 mm was also obtained as a structural reference to provide a qualitative indication of distortion correction accuracy. We also acquired a high-resolution T1-weighted 3-D turbo field echo inversion recovery image (repetition time ≈ 2000 msec, echo time = 3.9, inversion time = 1150 sec, flip angle = 8°, 256 × 205 matrix reconstructed to 256 × 256, reconstructed resolution = 0.938 × 0.938 mm, slice thickness = 0.9 mm, SENSE factor = 2.5), with 160 slices covering the whole brain, for purposes of high-precision construction of anatomically based ROIs (see below).

Distortion Correction

The spatial remapping correction was computed using the method reported elsewhere (Embleton et al., 2010; Visser et al., 2010). Briefly, the correction relied on the acquisition of two images for each slice and diffusion gradient orientation that were identical except for positive or negative blipped gradient polarity. The two images within each pair showed equal degrees of distortion along matching phase encode direction profiles (in the left–right direction), although distortion occurred in opposite directions (left to right or right to left). By integrating the signal from corresponding profiles in the phase encode direction, matching cumulative intensity values could be found and the correct position of this intensity determined as the mean of the positions from the two cumulative distorted profiles. A single-subject example of an uncorrected axial $b = 0$ image, positioned at the level of the magnetic susceptibility artifact in the temporal lobe, is provided in the supplementary information along with a fractional anisotropy map from the same subject and at the same slice that was calculated following the distortion correction (see Supplementary Figure S1a and b).

Temporal Lobe Regions

Temporal lobe regions, from which probabilistic tractography was initiated, were drawn on each subject's T1-weighted anatomical image using MRIcro (www.sph.sc.edu/comd/rorden/). A total of 14 temporal lobe regions consisted of three sets, each defined within either a rostral, mid, or more caudal cross-section of the left temporal lobe. To ensure the most consistency possible in the location of these regions across subjects, these cross-sections were identified in each subject's scan on the basis of common structural landmarks as follows. First, the pitch of the 3-D scan was rotated around the anterior commissure by 20°. These images were originally acquired so that they were axially coplanar with the AC–PC line. This rotation was performed so that they became axially coplanar with the longitudinal (rostral–caudal) axis of the temporal lobe (e.g., the length of the STS), so that coronal cross-sections would be perpendicular to this axis. The position of the rostral cross-section was identified by selecting the coronal slice that was 10 mm back from the most anterior tip of the left temporal lobe. The position of the caudal cross-section was the coronal slice at which the inferior aspect of the superior cerebellar peduncle meets the posterior wall of the pons (within the fourth ventricle). The slice that fell halfway between these positions was used as the mid cross-section and was invariably at the site of the basal artery as it ascends near the anterior surface of the brainstem. Examples of these slice positions can be seen in Figure 1A. Each of the cross-sections was extended by inclusion of three additional coronal slices that were taken rostrally in the case of the middle and posterior cross-sections and caudally in the case of the anterior cross-section. This meant that the thickness of each cross-section (corresponding to the *y* axis) was approximately equal to two voxels in the diffusion weighted images.

Once a cross-section was defined, the white matter of each of its constituent temporal gyri was delineated as a separate ROI. In the rostral cross-section, the regions included the white matter of the ventromedial gyrus of the temporal pole, the lateral gyrus of the temporal pole, and the superior (or dorsomedial) gyrus of the temporal pole. In the mid and caudal cross-sections, regions included the white matter of the parahippocampal gyrus, the fusiform gyrus, the inferior temporal gyrus, the middle temporal gyrus, and the superior temporal gyrus. The caudal cross-section also included a region that corresponded to the white matter of Heschl's gyrus.

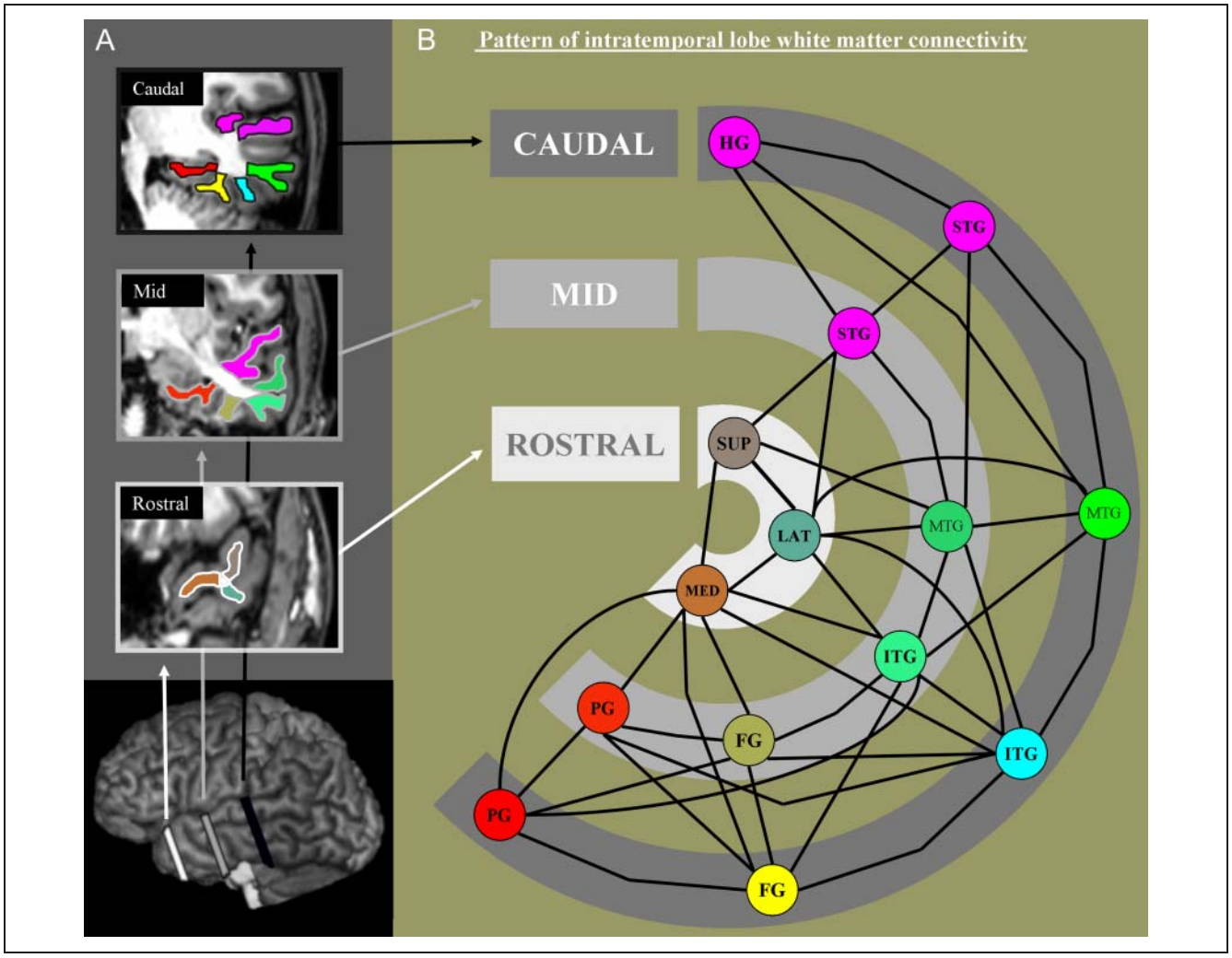

Figure 1. Intrarostral temporal lobe connectivity. (A) Single-subject example of the 14 temporal lobe seed/target regions used for probabilistic tractography. Connecting lines illustrate white matter pathways between pairs of regions detected in the thresholded connectivity matrix (see main text for details). (B) Summary of intratemporal lobe connectivity in the human brain as revealed by tractography. Each coronal cross-section is represented by an arc. The temporal lobe areas within each cross-section are represented by circles (see A for an anatomical reference). SUP = superior; LAT = lateral; MED = medial; PG = parahippocampal gyrus; FG = fusiform gyrus; ITG = inferior temporal gyrus; MTG = middle temporal gyrus; STG = superior temporal gyrus; HG = Heschl's gyrus. See also Supplementary Figure S1.

Each region was individually marked as follows. The gyral white matter was delineated from that of the temporal stem by a line drawn between the fundi of each adjacent sulcus. All gyral tissue within this boundary was then marked. This process was repeated on all four slices of the cross-section, resulting in a three-dimensional seed mask. This was subsequently treated with a scaled image intensity filter (minimum threshold, 158; maximum threshold, 254; threshold range, 0–254) to ensure that only white matter voxels were included (see Figure 1B).

We note here that our caudal-most regions did not correspond to those areas traditionally considered posterior temporal cortex, especially in the domain of language research (e.g., Hickok & Poeppel, 2007). Instead, this study focussed on the rostral half of the temporal lobe given that (a) contemporary functional neuroimaging, TMS, and neuropsychological studies clearly implicate anterior temporal areas in semantic and language processing yet the underlying connectivity of these areas has not been formally explored in the human and (b) because a considerable number of prior tractography studies have already explored the connectivity of the posterior-most temporal cortices (Rilling et al., 2008; Saur et al., 2008; Parker et al., 2005). Our caudal-most cross-section was defined according to a common anatomical landmark to maximize consistency in the location of ROIs across subjects (see above). Landmarks, more posterior to that used in this study, are less easy to identify reliably in MRI scans.

Language Network Regions of Interest

An additional set of ROIs were defined for the purpose of extracting pathways between each of the temporal lobe regions (above) and classical language areas outside the

temporal cortex. These included (in the left hemisphere) BA 44 (pars opercularis), BA 45 (pars triangularis), BA 47 (pars orbitalis), BA 46 and BA 9 (together forming dorsolateral pFC), BA 39 (angular gyrus), and BA 40 (the inferior portion of which comprises the supramarginal gyrus) and were defined using the corresponding Brodmann gray matter masks provided in the Wake Forest University Pickatlas toolbox (Maldjian, Laurienti, Kraft, & Burdette, 2003). These masks are provided in standard stereotaxic space, according to the Montreal Neurological Institute (MNI) protocol and thus required transformation into each subject's native anatomical space.

Spatial Transformations

DARTEL (diffeomorphic anatomical registration through an exponentiated lie algebra; Ashburner, 2007) was used to improve intersubject registration and thus greater precision in anatomical localization and statistical sensitivity (Klein et al., 2009). All steps were performed using SPM8 software (Wellcome Trust Centre for Neuroimaging, London, UK). In the case of each subject, the rotated T1-weighted anatomical image was first registered to the $b = 0$ diffusion-weighted image using a six-parameter rigid body transform. This transform placed this anatomical image within the same space as the DWI data, so that this image could be used to estimate further transforms to warp data from the native diffusion space to MNI space and vice versa (see below). This transform was also used to register temporal lobe regions defined on the anatomical image to that subject's diffusion space (reslicing performed with nearest neighbor interpolation), so that they could be used to initiate tractography.

The coregistered T1-weighted anatomical image of each subject was then partitioned into gray matter, white matter, and cerebrospinal fluid brain tissue compartments using SPM8's "new segment" toolbox. Following this, we used the DARTEL toolbox implemented within SPM8 to create a gray and white matter templates derived from the segmented anatomical images of all of the subjects in our data set. The gray matter component of this group template was then registered to SPM8's gray matter probability map, which is in the MNI standard stereotactic space, by estimating a 12-parameter affine transform. In the process of creating the template brain, DARTEL also outputs "flow fields" for each subject, which contains the transform from the original T1 image space to that of the group template. Each subject's flow field was combined with the template-to-MNI transform using SPM8's deformation utility. The inverse of this combined transform was applied to the frontal and parietal ROIs generated in MNI standard space (see above). Subsequent reslicing using nearest-neighbor interpolation placed them in the subject's native space. Furthermore, the noninverted combined transform (using nearest neighbor interpolation) was used to warp probability tractography maps into MNI standard space to allow the averaging of corresponding maps for the purpose of visualizing group-level tractography results (see Figure 3).

Probabilistic Fiber Tracking

A whole-brain volume of probability density functions (PDFs) was generated by analyzing each subject's distortion-corrected (Embleton et al., 2010; Visser et al., 2010) DWI data set with constrained spherical deconvolution (Tournier et al., 2008) and model-based residual bootstrapping (Jeurissen et al., 2011; Haroon et al., 2009). The constrained spherical deconvolution algorithm resolves multiple intravoxel fiber orientations without any assumptions on the diffusion process and in the presence of realistic data noise, whereas the application of a bootstrapping technique to the output from this algorithm allows quantification of the uncertainty of the inferred fiber orientations. Therefore, PDFs describe the uncertainty in the orientation(s) of fiber populations within a voxel. The quality of the estimation of fiber orientations obtained from the constrained spherical deconvolution algorithm is improved by using b values approaching 2000 sec mm^{-2} (Tournier et al., 2008; Tournier, Calamante, & Connelly, 2007). However, increasing the b value also increases the susceptibility of the algorithm to noise and increases variance in the estimated orientations (Tournier et al., 2007, 2008). Therefore, to achieve a good orientation to noise ratio we opted for a b value of 1200 sec mm^{-2}. In the supplementary information, we have provided a quiver plot that shows a single-subject example of the intravoxel fiber orientations estimated by the constrained spherical deconvolution algorithm in this study (Supplementary Figure S1c).

We implemented unconstrained probabilistic tractography using the PICo software package (Parker & Alexander, 2005). We initiated 20,000 Monte Carlo streamlines from each voxel in each temporal, frontal, and parietal "seed" region. Streamlines were generated in subvoxel steps (0.5 mm), the PDF being randomly sampled at each step to provide the direction to proceed. Stopping criteria for the streamlines were set so that tracking terminated if pathway curvature over a voxel was greater than 180° or the streamline reached a physical path limit of 500 mm. Whole-brain probabilistic maps result from PICo containing estimates of the maximum probability of the reconstruction of a pathway between a given brain voxel and the seed region in the given data set (note that these estimates are not, therefore, indicative of the connection strength, which indeed, is not determinable using this technique).

Connectivity Matrices

A single whole-brain probabilistic map was generated for each of the 14 temporal lobe seed regions for each individual participant. These maps were used to create an

intratemporal lobe connectivity matrix, as follows. Each probability map was successively masked with each of the temporal lobe seed regions and the maximum value within each of these target regions was extracted. Thereby, in each instance, we extracted a single probability estimate of a pathway existing between each pair of regions. Each of these values was placed into a subject-specific matrix. Each corresponding value was then averaged across all participants, resulting in a single group connectivity matrix. This matrix contained two probability estimates for each pair of regions, given that tracking was performed in both directions (e.g., region A [seed] to region B [target] and region B [seed] to region A [target]). There was a high degree of reliability between the estimates obtained in each direction ($r^2 = .92$). Given this result and that it is not possible to infer directionality of tracts from DWI tractography, these pairs of values were treated as repeat measurements of the same estimate and were combined (effectively collapsing the matrix across the diagonal) to form a single estimate probability index for each pair of regions (range = 0–1). A second connectivity matrix was constructed for each subject that contained estimates of the probability of a pathway existing between each temporal lobe region and each of the extratemporal language areas. These estimates were obtained in a manner similar to that described above, using each of the language area masks to extract the maximum value in each of these regions from the probabilistic map generated for each temporal lobe region, and vice versa. Corresponding cell entries were averaged across all participants, resulting in a single group connectivity matrix. This matrix also contained two probability estimates for each pair of regions, given that tracking was performed in both directions (e.g., temporal region A [seed] to frontal/parietal region B [target], and frontal/parietal region B [seed] to temporal region A [target]). Again, there was a high degree of reliability between the estimates obtained in each direction ($r^2 = .91$), and as such, they were combined to form a single estimate probability index for each pair of regions (range = 0–1).

Finally, in the very same manner as above, a third group connectivity matrix was constructed that contained estimates of the probability of a pathway existing in each pair of the frontal and parietal regions. Here too there was a high degree of reliability between the two estimates obtained ($r^2 = .96$), and thus, they were combined to form a single estimate probability index for each pair of regions (range = 0–1). Each of these group-level connectivity matrices were subjected to a threshold to ensure that only connections with a high probability were considered. In prior probabilistic tractography experiments (Cloutman, Binney, Drakesmith, Parker, & Lambon Ralph, 2012), we have ascertained that the values within such connectivity matrices conform to a Poisson distribution. The λ value of the Poisson distribution identified was then used to determine a threshold value at $p = .05$, and across subjects this consistently fell between 2.5% and 5% of the total number of streamlines initiated from the seed. In line with this observation, we opted to threshold the connectivity matrices from the present experiment at either 2.5% or 5% (more stringent) of the total number of streamlines initiated.

RESULTS

Intratemporal Lobe Connections

The final group intratemporal lobe connectivity matrix is displayed in Table 1, with each entry representing the probability of a pathway between a given pair of temporal lobe regions and is summarized visually in Figure 1A. The connectivity architecture in this figure was reconstructed as follows. Each cross-section is represented by an arc that has been color coded to denote its position along the temporal lobe (dark gray = caudal, light gray = mid, white = rostral). Each region of gyral white matter within a cross-section is represented by a circle. Lines connecting pairs of regions were included where that pathway was detected by tractography following the application of a minimum probability threshold to the connectivity matrix; the minimum probability threshold in this figure was 2.5% of the total combined number of streamlines propagated from the two regions (the pathways detected at a more stringent threshold of 5% are displayed in Supplementary Figure S2; the patterns of connectivity are largely identical to those in Figure 1).

The intratemporal lobe connectivity data reveal two potential sources of information convergence: (1) there are strong components of longitudinally oriented connectivity with pathways coursing the length of each temporal gyrus and (2) there are multiple lateral pathways from each gyrus to its neighbors, not only within a cross-section but also "diagonally" to the neighbors in the adjacent cross-section. These patterns of connectivity will drive information convergence along two dimensions of the temporal lobe: laterally, with increasing convergence when moving away from both the most superior and the most ventromedial structures and toward the laterally situated middle temporal gyrus, and longitudinally, with increasing convergence toward the rostral end of the temporal lobe culminating in the temporal pole. It is also of potential functional significance that one can observe "edge effects" in the connectivity architecture; the most superior and medial regions have only one connected neighboring structure, which could limit the influence of other sources of information on the processing in these "edge" regions (see Discussion). As a consequence of this, their function is likely to be "purer" than that of the intermediary, more laterally situated gyri (e.g., middle temporal gyrus). This idea has been highlighted, within the comparative neurology literature, as one of the most important principles of the organisation of the cerebral cortex (Mesulam, 1998); its primary function being to protect the fidelity of sensory tuning within unimodal processing pathways.

Table 1. Group-level Intratemporal Lobe Connectivity Matrix

	Rostral			*Mid*					*Caudal*					
	Medial	*Lateral*	*Superior*	*PhG*	*FG*	*ITG*	*MTG*	*STG*	*PhG*	*FG*	*ITG*	*MTG*	*STG*	*HG*
Rostral														
Medial		**0.168**	**0.181**	**0.147**	**0.082**	**0.043**	0.011	0.003	**0.089**	**0.038**	**0.027**	0.015	0.001	0.001
Lateral			**0.183**	0.004	0.005	**0.072**	**0.089**	**0.049**	0.008	0.009	**0.042**	**0.069**	0.004	0.004
Superior				0.002	0.002	0.008	**0.033**	**0.051**	0.003	0.002	0.006	0.020	0.002	0.004
Mid														
PhG					**0.256**	0.010	0.001	0.001	**0.740**	**0.125**	**0.031**	0.001	<0.001	<0.001
FG						**0.255**	0.009	0.002	**0.202**	**0.232**	**0.208**	0.010	0.001	0.001
ITG							**0.319**	0.012	**0.035**	**0.100**	**0.398**	**0.192**	0.006	0.007
MTG								**0.257**	0.001	0.003	**0.052**	**0.125**	**0.036**	0.007
STG									0.002	0.005	0.011	0.020	**0.101**	**0.093**
Caudal														
PhG										**0.414**	0.024	0.001	0.001	0.001
FG											**0.145**	0.003	0.001	0.001
ITG												**0.278**	0.008	0.013
MTG													**0.172**	**0.031**
STG														**0.402**
HG														

Bold font indicates that the connection probability survived the 2.5% threshold (see main text). PhG = parahippocampal gyrus; FG = fusiform gyrus; ITG = inferior temporal gyrus; MTG = middle temporal gyrus; STG = superior temporal gyrus; HG = Heschl's gyrus.

All intratemporal connections will reflect a combination of short association U-shaped fibers and both long and short fibers of the middle longitudinal fasciculus (MdLF) and the inferior longitudinal fasciculus. The connections linking the sections of the parahippocampal gyrus most likely correspond to fibers of the inferior longitudinal fasciculus (Catani & de Schotten, 2008; Schmahmann et al., 2007). The connections along the superior temporal gyrus (and from Hechl's gyrus to the caudal superior temporal gyrus) are most likely achieved via fibers belonging to the MdLF (Makris et al., 2009; Schmahmann et al., 2007). The longitudinally oriented connectivity along the superior temporal gyrus diminishes anterior to the mid cross-section, probably reflecting the known bifurcation of MdLF fibers where a lateral subset of fibers extend to the temporal pole and medial fibers split off and course through the extreme capsule (EmC) to the pFC (also see the results regarding extratemporal connectivity; Schmahmann et al., 2007).

If the connectivity pattern is used as a proxy for information convergence, then it appears that information encoded in the posterior gyri is gradually converged along the longitudinal axis of the temporal lobe, reaching a limit at the temporopolar cortex, where information becomes maximally "mixed" and thus minimally associated with any one of the inputs.

Extratemporal Lobe Connections

The second aim of this study reflected the role that the temporal lobe plays in language. We mapped the white matter pathways linking the 14 different temporal lobe subregions with inferior frontal and parietal sites classically associated with language processing. The inferior prefrontal and parietal VOIs (see Figure 2B for an anatomical reference) corresponded to BA 44 (pars opercularis), BA 45 (pars triangularis), BA 47 (pars orbitalis), BA 46 and BA 9 (together forming dorsolateral pFC), BA 39 (angular gyrus), and BA 40 (supramarginal gyrus). The extratemporal lobe connectivity matrix is summarised in Table 2 and illustrated in Figure 2A.

Figure 2A shows all of the temporal lobe regions in the same arrangement as Figure 1B but without the intratemporal pathways. The frontal and parietal regions are represented by boxes, each with a unique color. As before, lines connecting pairs of regions were included where

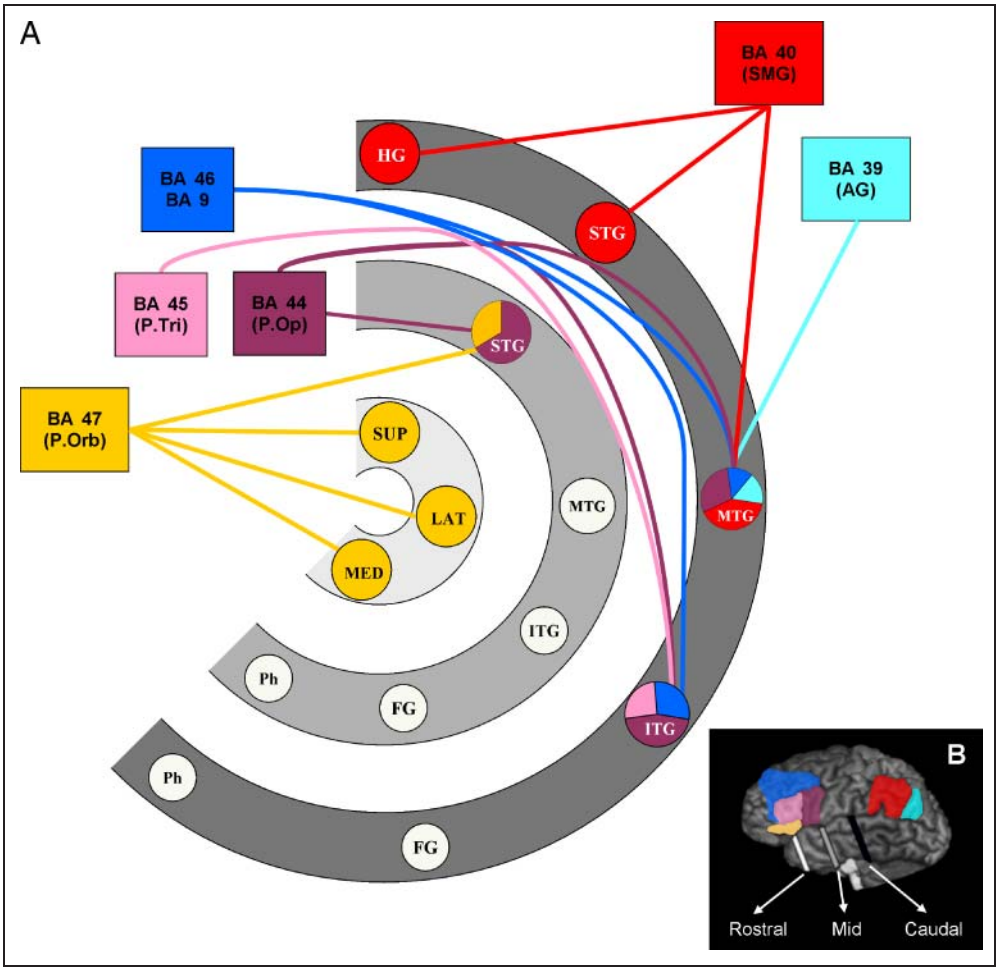

Figure 2. (A) Connectivity of the rostral temporal lobe to classical language areas in the frontal and parietal lobes. Temporal lobe areas are represented as circles that are arranged in the same manner as in Figure 1. The frontal and parietal language areas are represented by boxes, each with a unique color (see B for a color-matched anatomical reference). Only pathways between a temporal lobe area and a frontal or parietal area that were detected after the application of a 5% minimum probability of connection threshold (see main text) are shown and are represented by connecting lines. The pie charts display the relative proportion or balance of connectivity of the frontal/parietal regions to each of the temporal areas. BA = Brodmann's area; p.Orb = pars orbitalis; p.Tri = pars triangularis; P.Op = pars opercularis; SMG = supramarginal gyrus; AG = angular gyrus; SUP = superior; LAT = lateral; MED = medial; PG = parahippocampal gyrus; FG = fusiform gyrus; ITG = inferior temporal gyrus; MTG = middle temporal gyrus; STG = superior temporal gyrus; HG = Heschl's gyrus. See also Supplementary Figure S2.

Table 2. Group-level Extratemporal Lobe Connectivity Matrix

	Rostral			*Mid*					*Caudal*					
	Medial	*Lateral*	*Superior*	*PhG*	*FG*	*ITG*	*MTG*	*STG*	*PhG*	*FG*	*ITG*	*MTG*	*STG*	*HG*
Frontal														
BA 44	0.006	0.014	0.009	0.001	0.003	0.034	0.022	**0.140**	0.001	0.002	**0.101**	**0.127**	0.029	0.029
BA 45	0.004	0.004	0.014	0.001	0.002	0.014	0.009	0.026	0.002	0.003	**0.057**	0.031	0.006	0.010
BA 46 + BA 9	0.006	0.010	0.004	0.002	0.003	0.025	0.008	0.008	0.004	0.002	**0.065**	**0.057**	0.006	0.007
BA 47	**0.237**	**0.075**	**0.471**	0.014	0.004	0.012	0.016	**0.070**	0.008	0.008	0.025	0.028	0.006	0.011
Parietal														
BA 39	0.008	0.011	0.005	0.003	0.013	0.036	0.021	0.033	0.006	0.027	0.047	**0.071**	0.036	0.017
BA 40	0.004	0.013	0.004	0.001	0.002	0.025	0.018	0.015	0.001	0.001	0.042	**0.174**	**0.219**	**0.234**

Bold font indicates that the connection probability survived the 5% threshold (see main text). BA = Brodmann's area; PhG = parahippocampal gyrus; FG = fusiform gyrus; ITG = inferior temporal gyrus; MTG = middle temporal gyrus; STG = superior temporal gyrus; HG = Heschl's gyrus.

the value in the connectivity matrix exceeded a minimum probability threshold; a threshold of 5% of the total number of streamlines propagated from the two regions was applied in the generation of this figure. This higher threshold has been presented in this figure for the sake of clarity and the results obtained when using the 2.5% threshold were basically the same (displayed in Supplementary Figure S3). Where a temporal lobe region was demonstrated to have pathways interconnecting it with one or more of the frontal/parietal areas, we superimposed a pie chart that represents the relative proportion of streamlines visiting each of the frontal/parietal regions.

As can be seen in Figure 2A, in contrast to the graded and diffuse nature of the intratemporal pathways, our tractography results revealed that the temporal lobe areas exhibit more regionally distinct patterns of connectivity to the frontal/parietal areas. These patterns dissociate between the rostral, mid, and caudal temporal subregions and can be attributed to three well-known association tracts projecting to/from the temporal lobe (see Figure 3 and Movie S1). The three temporopolar areas shared a pathway exclusively with the pars orbitalis (BA 47) via the uncinate fasciculus (UF), which hooks behind the limen insulae to link the temporal pole and ventral pFC (gold tract in Figure 3; see also Gloor, 1997). Previous descriptions of the UF are consistent with our tractography results; in the temporal pole, fibers enter the UF from ventromedial, inferolateral, and superior lateral temporal cortices and link to BA 47, as well as BA 10, BA 11, BA 12, BA 13, BA 14, and BA 25, but not BA 45 or BA 44 (Schmahmann et al., 2007).

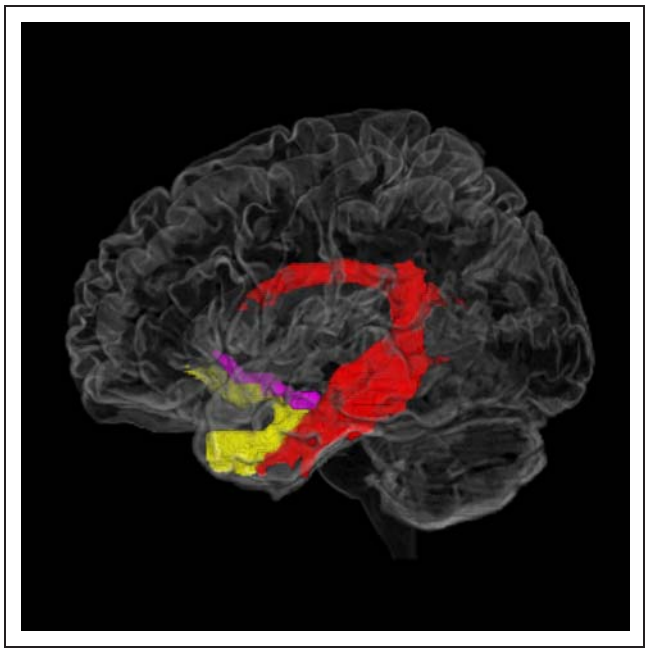

Figure 3. Three white matter tracts connecting the temporal lobe to the fronto-parietal language network. Three-dimensional representation of the three major association pathways projecting from the temporal lobe to the fronto-parietal language network. Tract reconstructions are based on the present tractography results. See also Movie S1.

In the mid temporal cross-section, at the 5% probability threshold, only the superior temporal gyrus was found to share a pathway with the frontal/parietal regions. Rostrally orientated projections connect mid superior temporal gyrus primarily with BA 44 and, to a more limited degree, BA 47 as well, via the EmC complex. The EmC complex courses between the insula and the claustrum connecting temporal to ventral and lateral prefrontal cortices and is consisted of fibers belonging to the uncinate (gold tract in Figure 3) and inferior fronto-occipital fasciculi (denoted in violet in Figure 3; see also Schmahmann et al., 2007; Gloor, 1997), the latter being that which the tractography results are most likely attributed to. In stark contrast, despite considerable intratemporal connectivity, the remaining areas within the mid temporal cross-section (the basal temporal region) failed to demonstrate any direct connections to the frontal and parietal VOIs.

Two areas within the caudal temporal cross-section exhibited a pathway to the pFC. Consistent with previous tractography studies (Frey, Campbell, Pike, & Petrides, 2008; Saur et al., 2008; Parker et al., 2005), our results identified pathways connecting the caudal middle temporal gyrus with posterior ventrolateral pFC (BA 44; pars opercularis) and dorsolateral pFC (BA 46/BA 9), which appear to be attributable to the arcuate fasciculus (AF; shown in red in Figure 3). There were also pathways connecting the caudal inferior temporal gyrus with BA 44, BA 45, and dorsolateral pFC (BA 46 and BA 9). These pathways also appear to be attributable to fibers of the AF (see Figure 3). Our results also revealed pathways connecting a number of caudal temporal areas with inferior parietal cortex. Heschl's gyrus and the caudal superior and middle temporal gyri exhibited pathways to the supramarginal gyrus (BA 40) mediated via fibers belonging to either the arcuate bundle or the MdLF. At the 5% matrix threshold, only the caudal middle temporal gyrus was found to have a pathway to the angular gyrus (BA 39). As with the mid temporal cross-section, the tractography results did not reveal pathways between the caudal ventral temporal areas and the frontal or parietal cortices.

These results cannot simply be driven by anatomical proximity given the following observations. First, in addition to shorter pathways (e.g., between posterior temporal cortices and inferior parietal sites) we observed long-range pathways (e.g., between the posterior temporal cortices and prefrontal cortices) with comparable probability estimates. Second, regions directly adjacent to each other (e.g., pars orbitalis, pars triangularis and pars opercularis) exhibited distinct patterns of connections with the temporal lobe. Aside from this, it is also interesting that the pars triangularis appears to have limited connectivity to the temporal lobe relative to its neighboring structures (see also Embleton, 2008). This might follow if the region plays an intermediary or transitional role between the pars orbitalis and pars opercularis. Similar notions have been proposed

Table 3. Group-level Fronto-parietal Connectivity Matrix

	Frontal				*Parietal*	
	BA 44	*BA 45*	*BA 46 + BA 9*	*BA 47*	*BA 39*	*BA 40*
Frontal						
BA 44		**1**	**0.988**	**0.853**	0.048	**0.250**
BA 45			**1**	**0.999**	0.026	0.037
BA 46 + BA 9				**0.523**	**0.066**	**0.251**
BA 47					0.028	0.015
Parietal						
BA 39						**0.998**
BA 40						

Bold font indicates that the connection probability survived the 5% threshold (see main text). BA = Brodmann's area.

on the basis of functional neuroimaging and TMS data (Gough, Nobre, & Devlin, 2005; Devlin, Matthews, & Rushworth, 2003).

Fronto-parietal Connections

Although it was not one of the core objectives of the current study, for completeness, we also extracted probability values for pathways between the frontal and parietal ROIs. The final fronto-parietal connectivity group matrix is displayed in Table 3, with each entry representing the probability of a pathway between a given pair of regions. For interpretation, we applied the more stringent 5% threshold to this matrix such that only pathways with a high probability were considered (values in bold font in Table 3). A visual summary of the matrix at the 5% threshold is provided in Figure S3.

Within each lobe (frontal and parietal) all of the ROIs were revealed to be interconnected with no exceptions. Interlobular connectivity was more regionally selective. The angular gyrus (BA 39) exhibited a pathway exclusively to/from dorsolateral pFC (BA 46 and BA 9) that is likely attributable to the superior longitudinal fasciculus. The supramarginal gyrus (BA 40) was found to share a pathway (attributable to fibers of the AF) with both dorsolateral pFC (BA 46 and BA 9) and pars opercularis (BA 44) of the frontal operculum. These results are consistent with those of other studies examining more detailed connectivity of the inferior parietal lobe using DWI tractography (Caspers et al., 2011).

DISCUSSION

In the following sections, we shall discuss both the intra- and extratemporal lobe "connectivity" in two steps. First, we shall discuss the direct implications of this novel neuroanatomical data, and then we shall provide a cognitive interpretation that will be related to hypotheses derived from prior functional data, patient studies, and computational modeling studies.

White Matter Connectivity within the Rostral Human Temporal Lobe

Our probabilistic tractography results suggest three key patterns of intratemporal lobe connectivity. First, there is strong longitudinally oriented connectivity along each temporal gyrus. Second, there are lateral connections within each cross-section between each gyrus and its neighboring gyri. Third, there are multiple instances where a gyrus shares a "diagonal" (both lateral and longitudinal) pathway with its neighbor in the adjacent cross-section. Overall, these results paint a picture of the temporal lobe as a highly convergent system that promotes integration of sensory processing streams simultaneously (i) along a longitudinal axis toward the rostral temporal lobe and (ii) laterally toward the inferolateral cortices.

Both the longitudinal (caudal → rostral) and lateral convergence principles are recognized within the neurological and neuroscience literatures. In sensory neuroscience, a hierarchical organization of convergence that proceeds rostrally up the temporal lobe is believed to underpin tuning of neuronal responses toward complex stimuli and away from low-level sensory variation (Rauschecker & Scott, 2009; Stringer & Rolls, 2002). Furthermore, the neuropsychological data points to a convergence of modality-specific processing streams toward the rostral temporal lobe in that posterior temporal lobe lesions are associated with modality-specific disorders (e.g., pure word deafness or visual agnosia; Karnath, Ruter, Mandler, & Himmelbach, 2009; Griffiths, 2002) while anterior temporal lobe damage is associated with pan-modal comprehension impairments (as found in semantic dementia; Bozeat, Lambon Ralph, Patterson, Garrard, & Hodges, 2000).

The evidence for lateral convergence of modality-specific processing streams stems from the comparative neurological literature. Connectivity data from the nonhuman primate indicate that visual and auditory association cortices project laterally to the STS (Seltzer & Pandya, 1978) and the status of the STS as polysensory association cortex has been confirmed by its responsiveness to visual, auditory, and somatosensory stimuli (Poremba et al., 2003; Bruce, Desimone, & Gross, 1981). In comparing functional data from the human and primate brain, Binder, Desai, Graves, and Conant (2009) noted the striking similarities and suggested that the human middle temporal gyrus and primate STS are homologues (also see below).

These two notions are, however, usually discussed in isolation and thus can appear to represent opposing theories for the mechanisms underlying cross-modal integration. Our tractography results, on the other hand, have shown for the first time that these two mechanisms exist in parallel within the human temporal lobe. Furthermore, these hypotheses have arisen primarily out of nonhuman

primate research and much of what is thought to be known about the finer details of connectivity in the human brain is based upon cross-species generalizations (Gloor, 1997). The validity of such generalizations is often assumed or justified on the basis of cytoarchitectural or functional equivalencies of regions (e.g., Ding, Van Hoesen, Cassell, & Poremba, 2009; Gloor, 1997). Despite similarities, however, there are undeniably morphological differences between the nonhuman primate and human temporal cortex (e.g., the absence of a homologue of the human middle temporal gyrus) and this, in addition to any impact there may have been of the evolution of language, is reason enough to suspect there may also be differences in the functional topology of the region and the underlying connectivity. Hence, in mapping fiber pathways of the human temporal lobe in vivo for the first time, we have also provided novel evidence in favour of the existence of both longitudinal and lateral convergence in the temporal lobe.

Cognitive Interpretation of the Intratemporal Lobe Connectivity

In Figure 4B, we display a sketch based on a flattened map of the temporal lobe with two principal sensory inputs (audition is represented in yellow and vision is represented in blue). Here we illustrate, using color mixing, the convergence of sensory information that we hypothesize to arise from the two conjoint principles of convergence suggested by the tractography results: (a) longitudinal and (b) lateral. This is as follows: in the caudal regions, fidelity of information to its original modality is maintained closest to its input (the aforementioned "edge effects"; see Results), but information is transmodal (mixed) within the inferior temporal gyrus/middle temporal gyrus. This convergence of information, however, is increasingly higher-order toward the more rostral regions at the limits of which information is maximally converged irrespective of the specific gyrus.

Figure 4B is remarkably consistent with the results of a recent meta-analysis of 120 functional neuroimaging studies of semantic processing (Binder et al., 2009), which, as can be seen in Figure 4C, implicated the middle temporal gyrus, right along from the angular gyrus to the temporal pole. Moreover, we recently conducted a functional magnetic resonance study where we compared semantic activation associated with verbal stimuli and nonverbal stimuli (Visser, Jefferies, Embleton, & Lambon Ralph, 2012). A conjunction analysis was performed to assess semantic activation common to the two tasks. As can be

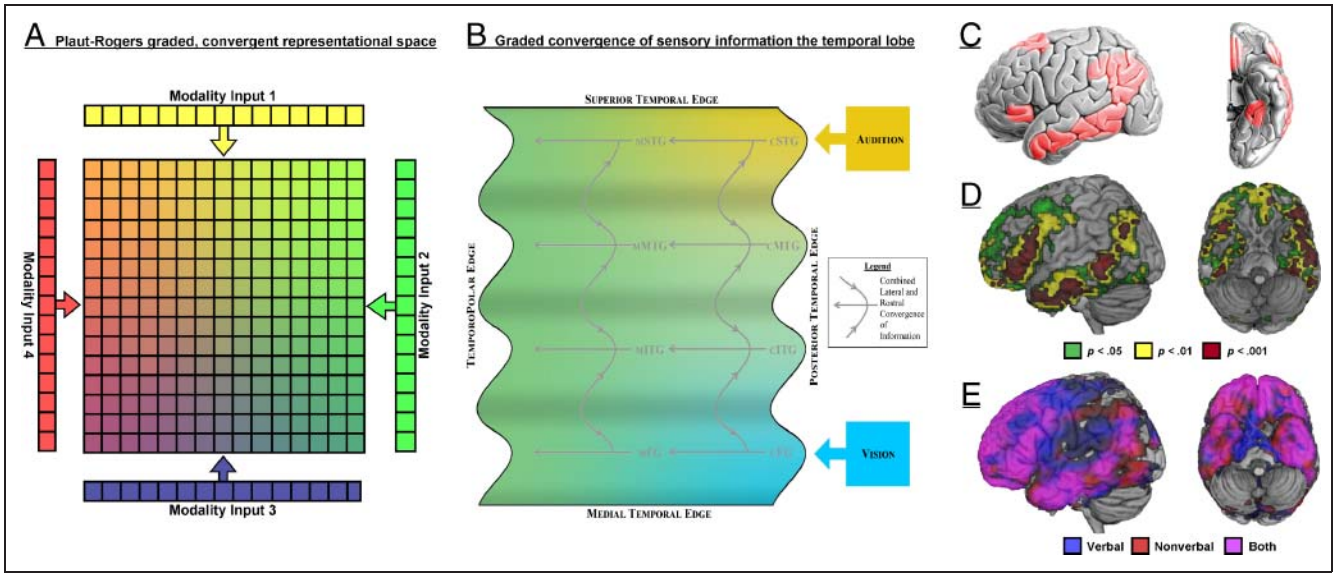

Figure 4. Information convergence in the rostral temporal lobe. (A) The graded representational space that emerged from differential connectivity of units to modality-specific inputs in the computational model of semantics implemented by Plaut (2002). Color mixing is used to represent the transition from unimodal processing at peripheral units to transmodal processing toward the center of the representational space. (B) This illustration represents a flattened map of the rostral temporal lobe with two principal inputs (audition and vision). Color mixing represents the convergence of information that is hypothesized to emerge on the basis of the two principal forms of convergence suggested by the tractography results: (i) caudal → rostral and (ii) lateral. (C) Lateral and ventral views of the left hemisphere semantic system identified in a recent meta-analysis of 120 functional neuroimaging studies (Binder et al., 2009; figure reproduced with kind permission of the authors). Note the similarities to the convergence hypothesized on the basis of the present tractography results as depicted in B and the functional data displayed in D. (D) Results of a conjunction analysis (Visser & Lambon Ralph, 2011) performed on functional MRI data to reveal activation common to semantic processing in the verbal domain and that in the nonverbal domain (i.e., pan-modal semantic activation). Rendered activation maps resulting from three different thresholds are superimposed over one another (see legend in the figure). Note the similarities to the semantic regions highlighted in B and C. (E) Overlaid beta-coefficient maps from a random effects analyses contrasting (i) the nonverbal semantic task versus a visual nonsemantic control task (red) and (ii) the verbal semantic task vs. a control task (blue). The pink color indicates an overlap of activation across the two tasks and thus highlights brain areas exhibiting pan-modal semantic activation. Note the similarities to the convergence of information that is hypothesized on the basis of the present tractography results as depicted in B.

seen in Figure 4D, this analysis revealed a cluster of common semantic activation in the temporal lobe that is identical to the region highlighted by Binder et al.'s (2009) meta-analysis (Figure 4C). In Figure 4E, upon a rendered brain, we have overlaid the beta-coefficient maps from the random effects analyses contrasting (a) the nonverbal semantic task versus a visual nonsemantic control task (in red) and (b) the nonverbal semantic task versus a control task (in blue). The overlay shows as pink where there was overlap between the two tasks and thus pan-modal activation. Again, this is highly consistent with the present findings and the inferred convergence of information depicted in Figure 4B; the length of the middle temporal gyrus and the very rostral third of the temporal lobe are activated by a semantic task regardless of the stimulus domain (verbal or nonverbal) while, toward the posterior temporal lobe, the superior gyrus and the inferior temporo-occipital cortex are preferentially activated by the verbal and nonverbal semantic tasks, respectively (corresponding to the top right and bottom right corners of Figure 4B). Figure 4 (C, D, and E) additionally implicates the anteroventral temporal lobe in pan-modal semantic processing. This is of relevance to the extratemporal lobe connectivity results and thus we shall return to it later in the Discussion. Finally, we note a third principle of information convergence in the temporal lobe. As can be seen in Figure 1, both the lateral and longitudinal convergence principles apply (note in particular the "diagonal" pathways that are simultaneously lateral and longitudinal) throughout the entire temporal lobe. As a product of these conjoint principles and as illustrated within Figure 3B, we hypothesize that convergence in the temporal lobe emerges as a graded process. More specifically, we suggest that the temporal lobe underpins a representational space in which there is a continuous integrative transition away from sensory-specific processing at its peripheries and toward increasingly higher-order combinations of information within more neutrally located territory. A strikingly similar notion has been implemented in computational models of semantic memory. Plaut (2002) demonstrated that graded specialisation of a representational space is an emergent property of differential, graded connection strengths between modality-specific input regions and a transmodal association region (see Figure 4A). Processing in units at the periphery of the representational space was closely associated with the neighboring input sources. Toward the center of the space, where connection strengths were very similar, units were involved in mapping between all "sensory" inputs and thus had become transmodal (we have represented this transition in Figure 4A with color mixing). Our tractography findings suggest that in the human temporal lobe there is underlying connectivity that could drive the emergence of graded specialization much like that which demonstrated in Plaut's model.

In summary, the broader functional implications are as follows. A large proportion of the left temporal lobe appears to be involved in mapping multiple cross-modal associations but in a graded fashion. Peak levels of cross-modal integration arise (analogous to the center of the Plaut's representational layer) along the length of the inferolateral cortices (inferior temporal gyrus and middle temporal gyrus, plus perhaps the fusiform gyrus) and within the rostral most aspects of the temporal lobe. As noted above, these regions are implicated by multiple sources of neuroscience data in the domain of semantic processing (which necessitates high-order information convergence; Binney et al., 2010; Binder et al., 2009; Patterson et al., 2007). In contrast, processing in areas away from these peak regions should change in a gradual manner and correspond to specific intermodality interfaces.

As a final note for this section, we acknowledge that thus far we have delivered our interpretation of the results from what might appear to be a purely bottom–up perspective in that emphasis has been placed upon a working hypothesis regarding the mechanism (the connectivity patterns) driving the formation of transmodal representations in the rostral temporal lobe from modality-specific inputs in more posterior regions. However, as mentioned above, DWI tractography is blind to directionality. Therefore, our results are equally consistent with the idea that the rostral temporal lobe also has a divergent top–down effect on multiple, lower-level sensory regions. In line with contemporary theories that advocate a role of the rostral temporal lobe in semantic cognition, language processes, and top–down effects in perception (Holland & Lambon Ralph, 2010; Lambon Ralph et al., 2010; Liu, Agam, Madsen, & Kreiman, 2009; Patterson et al., 2007; Rogers, Lambon Ralph, Hodges, & Patterson, 2004; Patterson & Lambon Ralph, 1999), we suggest that the bottom–up and top–down pathways co-exist dynamically; multi-modal perceptual input to the rostral temporal lobe is the basis for the encoding of semantic representations and, in turn, semantic representations influence processing of perceptual events in unimodal association cortices, thereby informing and guiding our interaction with objects, people and places.

Temporal Lobe Connectivity to Frontal and Parietal "Language" Areas

An additional target of this study was to compare each of the 14 temporal lobe regions, systematically, in terms of the white matter pathways that link them with frontal and inferior parietal sites that are classically associated with language processing. The results provide a more precise characterisation of the association fasciculi connecting the temporal lobe with frontal and inferior parietal cortices, beyond what has been described in prior DWI tractography studies, by means of identifying the specific temporal lobe sub-regions that are associated with each. Moreover, previous tractography studies have been primarily concerned with pathways mediating interactions between posterior temporal lobe (Wernicke's area) and frontal lobe regions

(i.e., Broca's area; Glasser & Rilling, 2008; Saur et al., 2008; Catani et al., 2005; Parker et al., 2005). To the best of our knowledge, no prior attempt has been made to use DWI tractography to compare the connectivity of the more rostrally situated temporal cortex to frontal/parietal language areas. Obtaining such information is essential given that anterior temporal semantic regions play a key role in comprehension and speech production (Schwartz et al., 2009; Patterson et al., 2007).

Overall, the extratemporal tractography results painted a very different picture to the graded intratemporal lobe connectivity. In contrast, there were four regionally distinct patterns, which dissociated between the left hemisphere rostral, mid, and caudal temporal lobe regions: (1) caudal lateral temporal regions were linked with inferior parietal and pFC via fibers of the MdLF and AF (red coded tract in Figure 3); (2) the mid superior temporal lobe was connected to ventrolateral pFC via the EmC complex (violet coded tract in Figure 3); (3) all three convolutions of the temporopolar cortex were exclusively connected to pars orbitalis and orbital cortex via the UF (gold-colored tract in Figure 3); and (4) there was a distinct "no-mans-land" in the anterior inferolateral and basal temporal cortex that exhibited an absence of connectivity to frontal and parietal regions in stark contrast to its high intratemporal lobe connectivity (see Figure 2). The inferred functional significance of these connectivity patterns depends largely on the function of the frontal and parietal areas, and in all cases, this is still debated. Below we shall give brief consideration to various possibilities.

The left AF has been the focus of, and successfully reconstructed within, numerous recent human tractography studies (Frey et al., 2008; Saur et al., 2008; Parker et al., 2005). It is regarded by classic anatomical models of language as the single most important pathway by which language information is transported from posterolateral temporal to inferior frontal language cortices (Geschwind, 1965). Our findings suggest that this direct pathway is predominately associated with the caudal middle temporal gyrus and inferior temporal gyrus in the temporal lobe, the dorsolateral frontal lobe, and the pars opercularis and pars triangularis of the frontal operculum. Pathways were also found to exist between the caudal temporal cortex and the angular and supramarginal gyri. This may form the caudal section of a recently proposed indirect pathway between the posterior temporal and prefrontal cortices that is relayed via the inferior parietal lobule (see also Frey et al., 2008; Catani et al., 2005; Parker et al., 2005). It has been suggested that the inferior parietal lobule could form a dynamic interface for sensory– and motor–speech systems at which feed-forward and feedback signals are compared and error corrected or minimized (Rauschecker & Scott, 2009).

The left hemisphere pathway connecting the superior temporal gyrus with the vlPFC via the EmC complex is consistent with the "ventral language route" that has been debated for over a century (Weiller, Bormann, Saur, Musso, & Rijntjes, 2011) but verified in a number of recent human tractography studies (Frey et al., 2008; Saur et al., 2008; Parker et al., 2005). Those and the present findings indicate that it, as part of the inferior fronto-occipital fasciculus, connects the auditory system in the superior temporal lobe to ventrolateral frontal cortices that are considered to serve in language production (i.e., Broca's area) but also cognitive control and selection processes (Devlin et al., 2003; Wagner, Paré-Blagoev, Clark, & Poldrack, 2001). It may be of significance that our intratemporal connectivity data indicates that sensory information is already highly converged at this superior middle temporal lobe subregion. Consequently, it is possible that semantic or other higher-order information (lexical and/or orthographical) can influence language production via this ventral pathway as opposed to the purely acoustic-motor mappings coded via the dorsal language pathway. Recent findings from intraoperative stimulation of the EmC complex and the speech errors generated by patients with damage to this region (Duffau, Gatignol, Moritz-Gasser, & Mandonnet, 2009; Schwartz et al., 2009; Lambon Ralph, McClelland, Patterson, Galton, & Hodges, 2001) support the notion of this type of division of labour in the language pathways (see Ueno, Saito, Rogers, & Lambon Ralph, 2011, for a recent computational implementation of the dorsal and ventral language pathways).

The function(s) of the UF is largely unknown and, moreover, is seldom discussed in the context of neurocognitive models of language. Its anatomy, however, has been extensively documented. As is consistent with our tractography results, it is described as directly connecting the temporopolar cortex with the ventrolateral, orbital, and polar frontal cortex via the temporal stem (Gloor, 1997). From this, we might infer at least two possibilities regarding its function. First, both the anterior temporal cortex (ATL; see below) and the ventrolateral pFC (Jefferies & Lambon Ralph, 2006; Devlin et al., 2003) have been implicated in semantic cognition and the UF may be responsible for mediating interactions between these structures. The second possibility is that, via the UF, the ATL receives behavioral- and emotion-related information from the orbital and medial frontal cortex (e.g., emotional valence: Levine, Katz, Dade, & Black, 2002), which would be consistent with the importance of the superior ATL in the processing of social concepts (Zahn et al., 2007). If this is correct, the temporopolar cortex would be yoked to a particular information source and, as a result, less multimodal than shown in Figure 4B. Consequently, following Plaut's computational implementation, the epicenter of the graded representational space might be a little more caudally situated, perhaps within the "no-mans-land" region observed in the anterior basal and inferolateral temporal cortex (see the next paragraph for further evidence in support of this hypothesis). These two hypotheses are not mutually exclusive and different pathways within the uncinate bundle may mediate both interactions.

It is striking and potentially important that a part of the highest-order convergence/association cortex (inferolateral and basal anterior temporal) has limited direct connectivity to regions outside the temporal lobe, as there is mounting evidence to suggest that this region is a core substrate of semantic memory (Visser & Lambon Ralph, 2011; Binney et al., 2010): (a) It is one of the most atrophied and hypometabolic areas in semantic dementia (Mion et al., 2010; Desgranges et al., 2007; Galton et al., 2001); (b) studies examining presurgical intracortical electrode recordings and event-related magneto-encephalography responses have found both auditory and visual responses in this area that appear to be related to semantic manipulations (Halgren et al., 2006; Marinkovic et al., 2003); (c) a number of PET-based neuroimaging studies of language function have also found activation of this region in response to both visually and aurally presented stimuli (Spitsyna, Warren, Scott, Turkheimer, & Wise, 2006; Sharp, Scott, & Wise, 2004; Noppeney & Price, 2002). Moreover, in recent distortion-corrected functional MRI studies (Visser et al., 2012; Visser & Lambon Ralph, 2011), we have shown that this region is activated by semantic tasks presented in both auditory vs. visual and verbal versus nonverbal domains providing further evidence for its role in supra-modal conceptual processing (see Figure 4D and E). Having such an arrangement of connectivity could be advantageous for the formation of coherent modality-invariant concepts (Lambon Ralph et al., 2010) and to isolate them from the direct influence of prefrontal control and/or context-coding systems. One high-profile computational model of semantic cognition was constructed so that semantic representations and context were coded on separate representational layers and isolated from each other by virtue of another intermediary layer (Rogers & McClelland, 2004). This circumvents the danger that information, which occurs in different contexts but for the same concept, is never converged within a unified semantic representation (e.g., birds both lay eggs and fly, but never at the same time—yet both features are core to the concept of birds). Our tractography results may have revealed a similar distinction in the human brain; the basal ATL may form the transmodal representational layer, whereas the superior temporopolar cortex, by virtue of connections with the frontal cortex, may act as an interface between this representational layer and control/context-coding prefrontal systems.

Acknowledgments

The authors would like to thank Karl Embleton and Hamied Haroon for their help with data acquisition and processing. This work was supported by Medical Research Council program grants (G0501632 and MR/J004146/1).

Reprint requests should be sent to Prof. Matthew A. Lambon Ralph, Neuroscience and Aphasia Research Unit (NARU), Zochonis Building, School of Psychological Sciences, University of Manchester, Oxford Road, Manchester, M13 9PL, UK, or via e-mail: matt.lambon-ralph@manchester.ac.uk.

REFERENCES

Ashburner, J. (2007). A fast diffeomorphic image registration algorithm. *Neuroimage, 38,* 95–113.

Binder, J. R., Desai, R. H., Graves, W. W., & Conant, L. L. (2009). Where is the semantic system? A critical review and meta-analysis of 120 functional neuroimaging studies. *Cerebral Cortex, 19,* 2767–2796.

Binney, R. J., Embleton, K. V., Jefferies, E., Parker, G. J. M., & Lambon Ralph, M. A. (2010). The ventral and inferolateral aspects of the anterior temporal lobe are crucial in semantic memory: Evidence from a novel direct comparison of distortion-corrected fMRI, rTMS, and semantic dementia. *Cerebral Cortex, 20,* 2728–2738.

Bozeat, S., Lambon Ralph, M. A., Patterson, K., Garrard, P., & Hodges, J. R. (2000). Non-verbal semantic impairment in semantic dementia. *Neuropsychologia, 38,* 1207–1215.

Bruce, C., Desimone, R., & Gross, C. G. (1981). Visual properties of neurons in a polysensory area in superior temporal sulcus of the macaque. *Journal of Neurophysiology, 46,* 369–384.

Caspers, S., Eickhoff, S. B., Rick, T., von Kapri, A., Kuhlen, T., Huang, R., et al. (2011). Probabilistic fiber tract analysis of cytoarchitectonically defined human inferior parietal lobule areas reveals similarities to macaques. *Neuroimage, 58,* 362–380.

Catani, M., & de Schotten, M. T. (2008). A diffusion tensor imaging tractography atlas for virtual in vivo dissections. *Cortex, 44,* 1105–1132.

Catani, M., Jones, D. K., & Ffytche, D. H. (2005). Perisylvian language networks of the human brain. *Annals of Neurology, 57,* 8–16.

Cloutman, L. L., Binney, R. J., Drakesmith, M., Parker, G. J. M., & Lambon Ralph, M. A. (2012). The variation of function across the human insula mirrors its patterns of structural connectivity: Evidence from in vivo probabilistic tractography. *Neuroimage, 59,* 3514–3521.

Deco, G., & Rolls, E. T. (2004). A neurodynamical cortical model of visual attention and invariant object recognition. *Vision Research, 44,* 621–642.

Desgranges, B., Matuszewski, V., Piolino, P., Chetelat, G., Mezenge, F., Landeau, B., et al. (2007). Anatomical and functional alterations in semantic dementia: A voxel-based MRI and PET study. *Neurobiology of Aging, 28,* 1904–1913.

Devlin, J. T., Matthews, P. M., & Rushworth, M. F. S. (2003). Semantic processing in the left inferior prefrontal cortex: A combined functional magnetic resonance imaging and transcranial magnetic stimulation study. *Journal of Cognitive Neuroscience, 15,* 71–84.

Ding, S., Van Hoesen, G. W., Cassell, M. D., & Poremba, A. (2009). Parcellation of human temporal polar cortex: A combined analysis of multiple cytoarchitectonic, chemoarchitectonic, and pathological markers. *The Journal of Comparative Neurology, 514,* 595–623.

Duffau, H., Gatignol, P., Moritz-Gasser, S., & Mandonnet, E. (2009). Is the left uncinate fasciculus essential for language? *Journal of Neurology, 256,* 382–389.

Dyrby, T. B., Søgaard, L. V., Parker, G. J., Alexander, D. C., Lind, N. M., Baaré, W. F. C., et al. (2007). Validation of in vitro probabilistic tractography. *Neuroimage, 37,* 1267–1277.

Embleton, K. V. (2008). *Studies of the neural basis of semantic memory: Application of distortion corrected fMRI and magnetic resonance diffusion imaging* [Thesis]. University of Manchester, UK.

Embleton, K. V., Haroon, H. A., Morris, D. M., Lambon Ralph, M. A., & Parker, G. J. M. (2010). Distortion correction for diffusion weighted MRI and tractography in the temporal lobes. *Human Brain Mapping, 31,* 1570–1587.

Felleman, D. J., & Van Essen, D. C. (1991). Distributed hierarchical processing in the primate cerebral cortex. *Cerebral Cortex, 1,* 1–47.
Frey, S., Campbell, J. S. W., Pike, G. B., & Petrides, M. (2008). Dissociating the human language pathways with high angular resolution diffusion fiber tractography. *Journal of Neuroscience, 28,* 11435–11444.
Galton, C. J., Patterson, K., Graham, K., Lambon-Ralph, M. A., Williams, G., Antoun, N., et al. (2001). Differing patterns of temporal atrophy in Alzheimer's disease and semantic dementia. *Neurology, 57,* 216–225.
Geschwind, N. (1965). Disconnexion syndromes in animals and man. *Brain, 88,* 585–644.
Glasser, M. F., & Rilling, J. K. (2008). DTI tractography of the human brain's language pathways. *Cerebral Cortex, 18,* 2471–2482.
Gloor, P. (1997). *The temporal lobe and the limbic system*. Oxford: Oxford University Press.
Gough, P. M., Nobre, A. C., & Devlin, J. T. (2005). Dissociating linguistic processes in the left inferior frontal cortex with transcranial magnetic stimulation. *Journal of Neuroscience, 25,* 8010–8016.
Griffiths, T. D. (2002). Central auditory processing disorders. *Current Opinion in Neurology, 15,* 31–33.
Halgren, E., Wang, C. M., Schomer, D. L., Knake, S., Marinkovic, K., Wu, J. L., et al. (2006). Processing stages underlying word recognition in the anteroventral temporal lobe. *Neuroimage, 30,* 1401–1413.
Haroon, H. A., Morris, D. M., Embleton, K. V., Alexander, D. C., & Parker, G. (2009). Using the model-based residual bootstrap to quantify uncertainty in fiber orientations from Q-ball analysis. *IEEE Transactions on Medical Imaging, 28,* 535–550.
Hickok, G., & Poeppel, D. (2007). The cortical organization of speech processing. *Nature Reviews Neuroscience, 8,* 393–402.
Holland, R., & Lambon Ralph, M. A. (2010). The anterior temporal lobe semantic hub is a part of the language neural network: Selective disruption of irregular past tense verbs by rTMS. *Cerebral Cortex, 20,* 2771–2775.
Jefferies, E., & Lambon Ralph, M. A. (2006). Semantic impairment in stroke aphasia versus semantic dementia: A case-series comparison. *Brain, 129,* 2132–2147.
Jeurissen, B., Leemans, A., Jones, D. K., Tournier, J., & Sijbers, J. (2011). Probabilistic fiber tracking using the residual bootstrap with constrained spherical deconvolution. *Human Brain Mapping, 32,* 461–479.
Jones, D. K., & Pierpaoli, C. (2005). *Contribution of cardiac pulsation to variability of tractography results*. Paper presented in the Proceedings of the Thirteenth Annual Meeting of the International Society of Magnetic Resonance in Medicine, Miami Beach, Forida.
Jones, E. G., & Powell, T. P. S. (1970). An anatomical study of converging sensory pathways within the cerebral cortex of the monkey. *Brain, 93,* 793–820.
Karnath, H. O., Ruter, J., Mandler, A., & Himmelbach, M. (2009). The anatomy of object recognition-visual form agnosia caused by medial occipitotemporal stroke. *Journal of Neuroscience, 29,* 5854–5862.
Klein, A., Andersson, J., Ardekani, B. A., Ashburner, J., Avants, B., Chiang, M. C., et al. (2009). Evaluation of 14 nonlinear deformation algorithms applied to human brain MRI registration. *Neuroimage, 46,* 786–802.
Klingler, J., & Gloor, P. (1960). The connections of the amygdala and of the anterior temporal cortex in the human brain. *Journal of Comparative Neurology, 115,* 333–369.
Lambon Ralph, M. A., McClelland, J. L., Patterson, K., Galton, C. J., & Hodges, J. R. (2001). No right to speak? The relationship between object naming and semantic impairment: Neuropsychological evidence and a computational model. *Journal of Cognitive Neuroscience, 13,* 341–356.
Lambon Ralph, M. A., Sage, K., Jones, R. W., & Mayberry, E. J. (2010). Coherent concepts are computed in the anterior temporal lobes. *Proceedings of the National Academy of Sciences, U.S.A., 107,* 2717–2722.
Levine, B., Katz, D. I., Dade, L., & Black, S. E. (2002). Novel approaches to the assessment of frontal damage and executive deficits in traumatic brain injury. In D. T. Stuss & R. T. Knight (Eds.), *Principles of frontal lobe function* (pp. 448–465). Oxford: Oxford University Press.
Liu, H. S., Agam, Y., Madsen, J. R., & Kreiman, G. (2009). Timing, timing, timing: Fast decoding of object information from intracranial field potentials in human visual cortex. *Neuron, 62,* 281–290.
Makris, N., Papadimitriou, G. M., Kaiser, J. R., Sorg, S., Kennedy, D. N., & Pandya, D. N. (2009). Delineation of the middle longitudinal fascicle in humans: A quantitative, in vivo, DT-MRI study. *Cerebral Cortex, 19,* 777–785.
Maldjian, J. A., Laurienti, P. J., Kraft, R. A., & Burdette, J. H. (2003). An automated method for neuroanatomic and cytoarchitectonic atlas-based interrogation of fMRI data sets. *Neuroimage, 19,* 1233–1239.
Marinkovic, K., Dhond, R. P., Dale, A. M., Glessner, M., Carr, V., & Halgren, E. (2003). Spatiotemporal dynamics of modality-specific and supramodal word processing. *Neuron, 38,* 487–497.
Mesulam, M. M. (1998). From sensation to cognition. *Brain, 121,* 1013–1052.
Mion, M., Patterson, K., Acosta-Cabronero, J., Pengas, G., Izquierdo-Garcia, D., Hong, Y. T., et al. (2010). What the left and right anterior fusiform gyri tell us about semantic memory. *Brain, 133,* 3256–3268.
Morán, M. A., Mufson, E. J., & Mesulam, M. M. (1987). Neural inputs into the temporopolar cortex of the rhesus monkey. *The Journal of Comparative Neurology, 256,* 88–103.
Noppeney, U., & Price, C. J. (2002). Retrieval of visual, auditory, and abstract semantics. *Neuroimage, 15,* 917–926.
Oldfield, R. C. (1971). The assessment and analysis of handedness: The Edinburgh inventory. *Neuropsychologia, 9,* 97–113.
Pandya, D. N., & Kuypers, H. G. J. M. (1969). Cortico-cortical connections in the rhesus monkey. *Brain Research, 13,* 13–36.
Pandya, D. N., & Seltzer, B. (1982). Association areas of the cerebral cortex. *Trends in Neurosciences, 5,* 386–390.
Parker, G. J. M., & Alexander, D. C. (2005). Probabilistic anatomical connectivity derived from the microscopic persistent angular structure of cerebral tissue. *Philosophical Transactions of the Royal Society of London, Series B, Biological Sciences, 360,* 893–902.
Parker, G. J. M., Luzzi, S., Alexander, D. C., Wheeler-Kingshott, C. A. M., Clecarelli, O., & Ralph, M. A. L. (2005). Lateralization of ventral and dorsal auditory-language pathways in the human brain. *Neuroimage, 24,* 656–666.
Patterson, K., & Lambon Ralph, M. A. (1999). Selective disorders of reading? *Current Opinion in Neurobiology, 9,* 235–239.
Patterson, K., Nestor, P. J., & Rogers, T. T. (2007). Where do you know what you know? The representation of semantic knowledge in the human brain. *Nature Reviews Neuroscience, 8,* 976–987.
Plaut, D. C. (2002). Graded modality-specific specialisation in semantics: A computational account of optic aphasia. *Cognitive Neuropsychology, 19,* 603–639.
Pobric, G., Jefferies, E., & Lambon Ralph, M. A. (2010). Category-specific versus category-general semantic impairment induced

by transcranial magnetic stimulation. *Current Biology, 20,* 964–968.
Poremba, A., Saunders, R. C., Crane, A. M., Cook, M., Sokoloff, L., & Mishkin, M. (2003). Functional mapping of the primate auditory system. *Science, 299,* 568–572.
Rauschecker, J. P., & Scott, S. K. (2009). Maps and streams in the auditory cortex: Nonhuman primates illuminate human speech processing. *Nature Neuroscience, 12,* 718–724.
Rilling, J. K., Glasser, M. F., Preuss, T. M., Ma, X. Y., Zhao, T. J., Hu, X. P., et al. (2008). The evolution of the arcuate fasciculus revealed with comparative DTI. *Nature Neuroscience, 11,* 426–428.
Rogers, T. T., Lambon Ralph, M. A., Hodges, J. R., & Patterson, K. (2004). Natural selection: The impact of semantic impairment on lexical and object decision. *Cognitive Neuropsychology, 21,* 331–352.
Rogers, T. T., & McClelland, J. L. (2004). *Semantic cognition: A parallel distributed processing approach*. Cambridge, MA: MIT Press.
Saur, D., Kreher, B. W., Schnell, S., Kummerer, D., Kellmeyer, P., Vry, M. S., et al. (2008). Ventral and dorsal pathways for language. *Proceedings of the National Academy of Sciences, U.S.A., 105,* 18035–18040.
Schmahmann, J. D., & Pandya, D. N. (2006). *Fiber pathways of the brain*. New York: Oxford University Press.
Schmahmann, J. D., Pandya, D. N., Wang, R., Dai, G., D'Arceuil, H. E., de Crespigny, A. J., et al. (2007). Association fibre pathways of the brain: Parallel observations from diffusion spectrum imaging and autoradiography. *Brain, 130,* 630–653.
Schwartz, M. F., Kimberg, D. Y., Walker, G. M., Faseyitan, O., Brecher, A., Dell, G. S., et al. (2009). Anterior temporal involvement in semantic word retrieval: Voxel-based lesion-symptom mapping evidence from aphasia. *Brain, 132,* 3411–3427.
Seltzer, B., & Pandya, D. N. (1978). Afferent cortical connections and architectonics of superior temporal sulcus and surrounding cortex in rhesus-monkey. *Brain Research, 149,* 1–24.
Sharp, D. J., Scott, S. K., & Wise, R. J. S. (2004). Retrieving meaning after temporal lobe infarction: The role of the basal language area. *Annals of Neurology, 56,* 836–846.
Spitsyna, G., Warren, J. E., Scott, S. K., Turkheimer, F. E., & Wise, R. J. S. (2006). Converging language streams in the human temporal lobe. *Journal of Neuroscience, 26,* 7328–7336.
Stringer, S. M., & Rolls, E. T. (2002). Invariant object recognition in the visual system with novel views of 3D objects. *Neural Computation, 14,* 2585–2596.
Tournier, J., Yeh, C., Calamante, F., Cho, K., Connelly, A., & Lin, C. (2008). Resolving crossing fibres using constrained spherical deconvolution: Validation using diffusion-weighted imaging phantom data. *Neuroimage, 42,* 617–625.
Tournier, J. D., Calamante, F., & Connelly, A. (2007). Robust determination of the fibre orientation distribution in diffusion MRI: Non-negativity constrained super-resolved spherical deconvolution. *Neuroimage, 35,* 1459–1472.
Tuch, D. S. (2004). Q-ball imaging. *Magnetic Resonance in Medicine, 52,* 1358–1372.
Ueno, T., Saito, S., Rogers, T. T., & Lambon Ralph, M. A. (2011). Lichtheim 2: Synthesizing aphasia and the neural basis of language in a neurocomputational model of the dual dorsal-ventral language pathways. *Neuron, 72,* 385–396.
Visser, M., Embleton, K. V., Jefferies, E., Parker, G. J., & Lambon Ralph, M. A. (2010). The inferior, anterior temporal lobes and semantic memory clarified: Novel evidence from distortion-corrected fMRI. *Neuropsychologia, 48,* 1689–1696.
Visser, M., Jefferies, E., Embleton, K. V., & Lambon Ralph, M. A. (2012). Both the middle temporal gyrus and the ventral anterior temporal area are crucial for multimodal semantic processing: Distortion-corrected fMRI evidence for a double gradient of information convergence in the temporal lobes. *Journal of Cognitive Neuroscience, 24,* 1766–1778.
Visser, M., & Lambon Ralph, M. A. (2011). Differential contributions of bilateral ventral anterior temporal lobe and left anterior superior temporal gyrus to semantic processes. *Journal of Cognitive Neuroscience, 23,* 3121–3131.
Wagner, A. D., Paré-Blagoev, E. J., Clark, J., & Poldrack, R. A. (2001). Recovering meaning: Left prefrontal cortex guides controlled semantic retrieval. *Neuron, 31,* 329–338.
Weiller, C., Bormann, T., Saur, D., Musso, M., & Rijntjes, M. (2011). How the ventral pathway got lost—And what its recovery might mean. *Brain and Language, 118,* 29–39.
Zahn, R., Moll, J., Krueger, F., Huey, E. D., Garrido, G., & Grafman, J. (2007). Social concepts are represented in the superior anterior temporal cortex. *Proceedings of the National Academy of Sciences, U.S.A., 104,* 6430–6435.